https://doi.org/10.5194/egusphere-2026-1707
Preprint. Discussion started: 14 April 2026

Spatiotemporal Linkage and Transmission of Urban Heat Islands in the Yangtze River Delta Urban Agglomeration: The Role of Urban Heat Advection

Jiesheng Xue[1], Yuanjian Yang[1*], Guoyu Ren[2], Simone Lolli[3]

[1]State Key Laboratory of Climate System Prediction and Risk Management, School of Atmospheric Physics, Nanjing University of Information Science & Technology, Nanjing 210044, China
[2]Department of Atmospheric Science, School of Environmental Studies, China University of Geosciences, Wuhan, 430070, China
[3]CNR-IMAA, Contrada S. Loja snc, Tito Scalo (PZ), 85050, Italy

Correspondence to: Yuanjian Yang (yyj1985@nuist.edu.cn)

Abstract. Urban heat islands (UHIs) substantially modify the urban thermal environment, yet the contribution of non-local processes such as urban heat advection (UHA) in dense urban agglomerations remains poorly quantified. Using five years of high-density automatic weather station data and Weather Research and Forecasting (WRF) simulations, we investigate how UHA links canopy-layer UHI (CUHI) and boundary-layer UHI (BUHI) across the Suzhou-Wuxi-Changzhou metropolitan area in the Yangtze River Delta, China. UHA exhibits pronounced spatiotemporal variability, systematically transporting heat from upwind to downwind cities along the prevailing winds. Under northwesterly flow, daily-mean UHA intensities increase from negative values in upwind regions to about 0.3 °C downstream, with nocturnal UHA during peak hours reaching roughly 0.6 °C. Observations show that nighttime UHA is nonlinearly modulated by wind speed and planetary boundary-layer height (PBLH), with maximum downstream warming under moderate winds and intermediate PBLH, whereas deep daytime convective boundary layers (PBLH ≥ 800 m) dilute urban heat plumes and can reverse UHA to a net cooling effect. WRF experiments further indicate that urbanization in the upstream city of Changzhou enhances CUHII in the adjacent downstream Wuxi by up to about 0.6 °C (9–42%) and BUHII by up to about 0.35 °C (19–141%), with detectable canopy-level warming extending beyond 100 km downwind. These results demonstrate that cross-city UHA superposition, strongly regulated by boundary-layer dynamics, is a key physical process coupling UHIs within urban agglomerations, requiring explicit consideration in regional climate assessments.

1 Introduction

The urban heat island (UHI) is one of the primary characteristics of anthropogenic impacts on local and regional urban climate (Oke et al., 2017). Urban expansion and anthropogenic heat emissions are key drivers of local temperature rise (Chen et al., 2022; Shi et al., 2024). Extensive studies have explored the spatial structure, temporal evolution, and physical mechanisms of UHI at the individual city scale (Oke, 1973; Phelan et al., 2015; Zhang et al., 2024a; Zheng et al., 2024). However, the rapid development of urban agglomerations in recent years and the consequent reduction in inter-city distances have substantially altered the regional thermal environment (Zhou et al., 2018). Considering the interactions between UHIs across adjacent cities

https://doi.org/10.5194/egusphere-2026-1707
Preprint. Discussion started: 14 April 2026

is therefore essential for a comprehensive understanding of the spatiotemporal evolution of the thermal environment within urban agglomerations.

The spatial influence extent of the UHI is governed by background meteorological conditions (Lowry, 1977; Stull, 1988). Under quiescent synoptic conditions, UHI-induced local circulation typically exhibits as an "urban thermal dome" structure, characterized by the most pronounced urban-rural thermal differences at the local scale (Oke et al., 2017). When regional background winds prevail, an "urban thermal plume" generates (Stull, 1988), transporting heat, moisture, and pollutants downstream (Brousse et al., 2022; Lowry, 1977; Moustaoui and Georgescu, 2025; Yang et al., 2023; Zhang et al., 2009). Early observations indicated that urban thermal plumes could extend 10–15 km downwind (Dirks, 1974; Wong and Dirks, 1978), while recent modelling results show significant heating up to 70 km downwind of the city (Cosgrove and Berkelhammer, 2018). The process of transporting heat to the downwind region of the UHI by horizontal winds is called urban heat advection (UHA); however, few studies have considered how horizontal wind fields alter the urban thermal environment through the advection-driven UHI component, or deemed this effect insignificant (Bassett et al., 2016). Ignoring the influence of UHA may lead to an underestimation of the actual impacts of urban heat on the region.

Current research on UHA primarily utilizes three observational approaches to collect urban temperature: fixed sensors at weather stations (Bassett et al., 2016, 2017), mobile sensors deployed on traverse vehicles (Danzig et al., 2025), and crowdsourced data from crowd weather stations (Kittner et al., 2025). Observations within the urban canopy can effectively capture the two-dimensional spatial patterns and extent of UHI-related UHA, but the paucity of high-quality, high-density urban observation networks constrains UHA studies (Bassett et al., 2016). Modelling methods can complement the spatial and temporal dimensions that observations cannot capture. For example, mesoscale numerical models (Bassett et al., 2019), Lagrange transport models (Cosgrove and Berkelhammer, 2018; Moustaoui and Georgescu, 2025), and urban micrometeorological models (Dinda and Chatterjee, 2022) have been applied to quantify UHA effects across local to mesoscale scales, thereby alleviating the vertical and coverage limitations of surface measurements. Consequently, combining high-resolution observations with mesoscale and urban numerical models has become a key approach for investigating UHA across local to regional scales.

UHA exerts a profound influence on the downwind thermal environment at the urban scale. For example, analyses of observation data show that UHA can affect ambient temperatures by up to 1°C in rural De Bilt (temperate maritime climate), Netherlands (Brandsma et al., 2003); the downwind warming in Birmingham (temperate maritime climate), UK can reach 1.2°C and extend beyond 10 km (Bassett et al., 2016); and downwind temperatures rise induced by UHA in Lubbock (semi-arid region), Texas can exceed 4°C (Danzig et al., 2025). The observational findings are corroborated by numerical simulation results; for example, downwind temperatures can be up to 2.5°C higher than upwind during a Birmingham heatwave event (Heaviside et al., 2015). UHA processes are influenced by meteorological conditions and underlying surface characteristics. Generally, the contribution of UHA to ambient temperature rise is most significant under moderate wind speeds, while the UHA effect is weaker under strong mesoscale forcing or calm conditions (Bassett et al., 2016; Kittner et al., 2025). However, current research often lacks consideration of the influence of more boundary layer conditions on UHA processes, such as

https://doi.org/10.5194/egusphere-2026-1707
Preprint. Discussion started: 14 April 2026

planetary boundary layer height (PBL), beyond conventional near-surface meteorological factors. Furthermore, the intensity and spatial extent of UHA are closely related to urban size (Bassett et al., 2019) and UHI intensity (Kittner et al., 2025). They are modulated by the spatial configuration or local climate zones of upwind cities (Bassett et al., 2016; Kittner et al., 2025), as well as by downwind land use types (e.g., downstream lakes can act as heat sinks for UHA and reduce the horizontal transport distance of heat plumes) (Cosgrove and Berkelhammer, 2018). It is noteworthy that even in small urban areas, UHAs can exacerbate air temperatures downwind (Bassett et al., 2017). However, existing UHA studies primarily focus on intra-city heat transport or the impact of isolated cities, neglecting the synergistic transport effects generated by dense heat sources within urban agglomerations. It remains an open question whether the cross-city superposition of UHAs from multiple cities within an urban agglomeration has become a critical physical process coupling the thermal environments of adjacent cities. The extent to which upwind UHAs exacerbate downstream UHI intensity is currently poorly understood.

The Yangtze River Delta (YRD) region in China exhibits a spatial pattern characterized by the clustered development of multiple metropolitan areas. To understand the processes of UHA, the UHI can be vertically delineated into the canopy-layer UHI (CUHI) and the boundary-layer UHI (BUHI) (Oke, 1976). Using high-density automatic weather station observations and WRF-SLUCM simulations over the YRD, we investigate how UHA links UHIs across cities within an urban agglomeration. Specifically, we address: (1) how CUHI and BUHI are coupled along the urban chain under different wind regimes; (2) how wind speed and PBLH modulate the intensity and diurnal asymmetry of UHA; and (3) to what extent upstream urbanization enhances downstream CUHII and BUHII and over what distances.

2 Data and methods

2.1 Study area and data

YRD is one of the most densely populated and economically developed regions in China. Driven by rapid population growth and high-speed economic development, the region has experienced extensive urban spatial expansion over recent decades (Shi et al., 2025; Tian et al., 2011). The Suzhou-Wuxi-Changzhou (SuXiChang) metropolitan area, consisting of the cities of Suzhou, Wuxi, and Changzhou, is one of the important urban agglomerations within the YRD (Fig. 1a and 1d), located in a subtropical monsoon climate zone. The urbanization process in this region has significantly intensified both the spatial extent and the intensity of UHI (Lu et al., 2018), consequently altering the regional thermal landscape pattern, such as the shrinking of thermal transition zones. As a result, this area is facing severe urban thermal environment risks.

Meteorological observations from automated weather stations, including air temperature, wind speed, and wind direction, were collected and quality-controlled from 2016 to 2020. Stations located within 1 km of large water bodies, or with elevations exceeding 100 m relative to the lowest station, were excluded to ensure environmental representativeness (Yao et al., 2023). Observation stations were further classified into urban and rural categories (Fig. 1b, Table S1), referring to anthropogenic heat flux (AHF) intensity (Fig. 1c) and built-up density (Fig. 1d). Specifically, urban stations (U1–U10) are characterized by densely built-up areas with high AHF intensity; whereas rural reference stations were matched according to the same latitudinal zone

https://doi.org/10.5194/egusphere-2026-1707
Preprint. Discussion started: 14 April 2026

as the urban areas, featuring low impervious surface coverage and flat topography. In addition, the wind directions selected for analysis should be filtered to avoid interference from large urban-derived heat in rural areas. Due to the aggregated development of urban agglomerations, area and station classifications in this study do not strictly adhere to administrative boundaries.

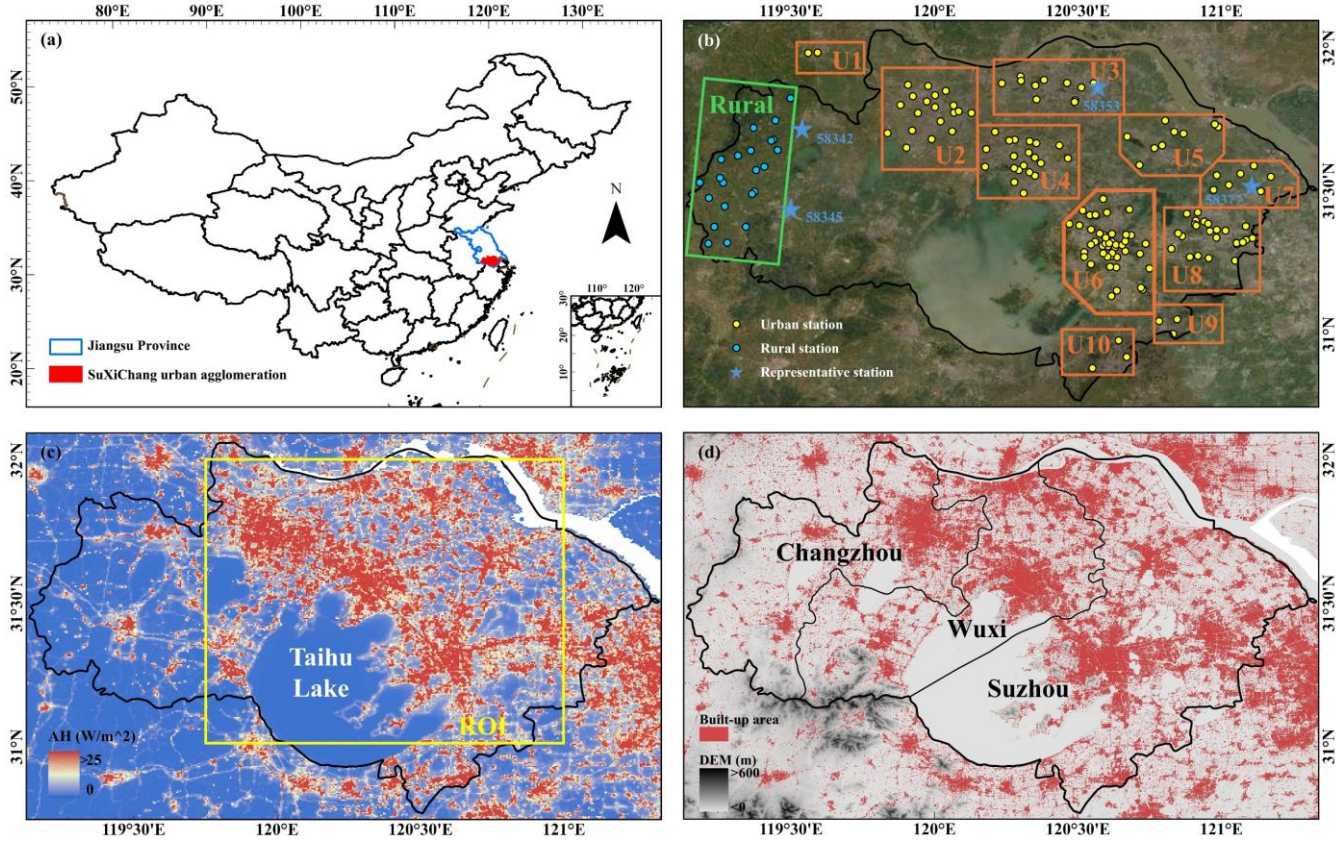

Figure 1. (a) Geographic location of the study area in China; (b) Locations of the automated weather stations, where the yellow and blue circles represent urban and rural stations, respectively, and blue asterisks indicate representative stations of the regional wind field. (c-d) Spatial distribution of (c) anthropogenic heat flux and (d) built-up areas within the SuXiChang area. The background in (b) is from the Esri World Imagery basemap as of 22 July 2020. The line in (c) represents the region of interest, and the lines in (d) represent the administrative boundaries of the three cities of Suzhou, Wuxi, and Changzhou.

In addition, PBLH data were obtained from a global continental dataset (Guo et al., 2024), which integrates high-resolution radiosonde measurements, ERA5 reanalysis, and Global Land Data Assimilation System (GLDAS) products through machine learning algorithms. This dataset has a 3-hourly temporal resolution and 0.25°×0.25° horizontal spatial resolution. The region of interest (ROI) was delineated based on the location of downtown areas of Changzhou, Wuxi, and Suzhou (represented by the U2, U4, and U6 stations, respectively), with a spatial extent of 31°N–32°N, 119.75°E–121°E, and covers 86.3% of the

https://doi.org/10.5194/egusphere-2026-1707
Preprint. Discussion started: 14 April 2026

urban meteorological stations included in the analysis (Fig. 1c). Grid data within the ROI were selected and spatially averaged based on prevailing wind direction to represent the PBLH over the core urban agglomeration region.

2.2 Methods

2.2.1 Calculation of CUHI intensity

The CUHI intensity (CUHII) was calculated by comparing air temperatures between urban and rural areas (Oke et al., 2017):

$$CUHII_i(t) = \bar{T}_i(t) - \bar{T}_r(t), \quad (1)$$

where $\bar{T}_i(t)$ is the average 2-meter temperature of all urban stations in region *i* (U1–U10) at time *t*, and $\bar{T}_r(t)$ is the average 2-meter temperature of all rural reference stations at the same time.

2.2.2 Calculation of UHA intensity

Four representative national meteorological stations (58342, 58345, 58353, 58377) were selected to calculate the regional wind direction and wind speed. These stations are located in relatively open surroundings, where observations are less disturbed by local surface heterogeneity, thereby providing more reliable representations of the regional-scale background wind field (Figure 1b).

Wind directions of representative stations were categorized into eight sectors with equal intervals of 45° to identify the daily prevailing wind direction. The quantification of UHA intensity was modified based on Bassett et al. (2016), with further consideration given to exclude seasonal signals:

$$UHA_i^{\theta}(t,s) = CUHII_i^{\theta}(t,s) - \overline{CUHII_i(t,s)}, \quad (2)$$

$$\overline{CUHII_i(t,s)} = \frac{\sum_{\theta=1}^{8} CUHII_i^{\theta}(t,s)}{8}, \quad (3)$$

where $CUHII_i^{\theta}(t,s)$ denotes the *CUHII* in region *i* under the prevailing wind direction θ during season *s*, while $\overline{CUHII_i(t,s)}$ represents the average CUHII across all wind directions in the same season *s*.

2.2.3 Model configuration

The spatial features of UHA were evaluated using the Weather Research and Forecasting (WRF) model, version 3.9.1, coupled with a single-layer urban canopy model (SLUCM). WRF-SLUCM can reasonably reproduce the intensity and spatiotemporal distribution of UHI (Zhu and Ooka, 2023). A triple-nested two-way domain configuration was employed, with the innermost domain (d03) encompassing the study area (Fig. 2a). The domains feature horizontal grid dimensions of 102 × 102, 160 × 130, and 286 × 160, with corresponding resolutions of 9 km, 3 km, and 1 km, and 36 vertically stretched non-uniform sigma levels. The main physical parameterization schemes adopted in this study include: the Thompson microphysics scheme (Thompson et al., 2008), the YSU planetary boundary layer scheme (Hong et al., 2006), the Goddard shortwave radiation scheme (Chou

https://doi.org/10.5194/egusphere-2026-1707
Preprint. Discussion started: 14 April 2026

and Suarez, 1994), the RRTM longwave radiation scheme (Mlawer et al., 1997), the unified Noah land surface model (Tewari et al., 2004), and the Eta Similarity surface layer scheme (Janjić, 1994). Initial and lateral boundary conditions were derived from the 6-hourly, 0.25° National Centers for Environmental Prediction (NCEP) Final Operational Global Analysis (FNL) data. The simulations in this study initiated at 08:00 local time on December 23, 2017, over a 48-hour period, and the first 24-hour spin-up period was applied for all simulations.

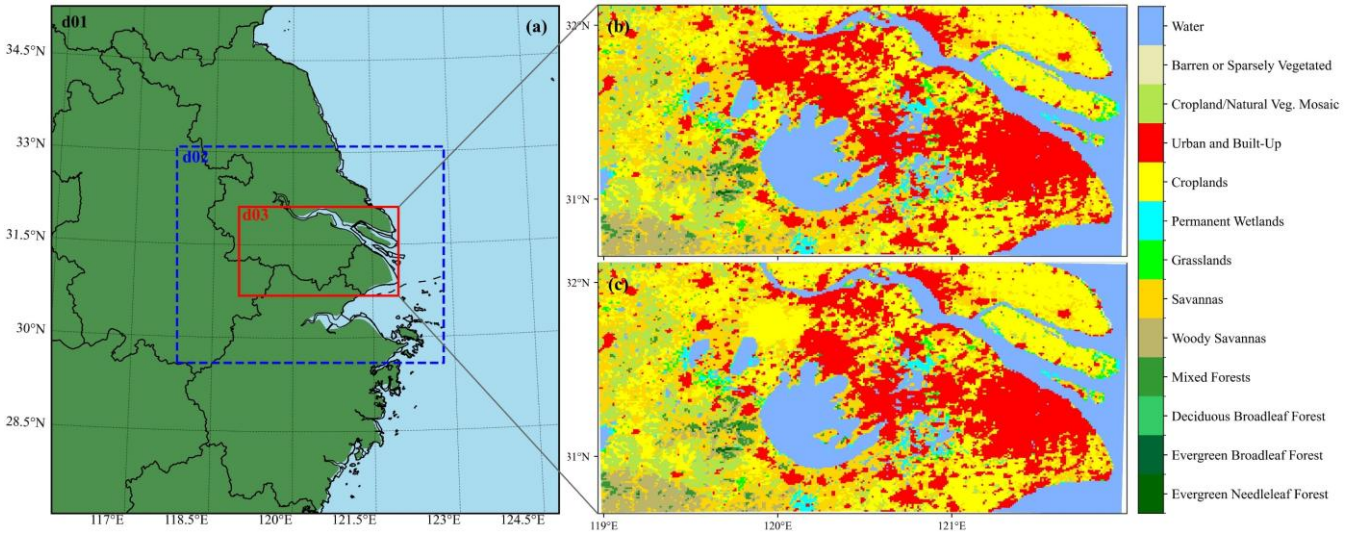

Figure 2. (a) The setup of the nested domain over the study area. Land use and land cover within the innermost domain for (b) control simulation and (c) sensitivity experiment.

The default land use/land cover (LULC) data within WRF was replaced with the MODIS land cover product (MCD12Q1, Version 6.1), which has a 500-m spatial resolution with better detail (Friedl and Sulla-Menashe, 2022). To quantitatively assess the contribution of the urban landscape to UHA, a sensitivity experiment (EXP) was conducted. In particular, the urban LULC within the downtown area of Changzhou city (represented by U2 stations) was replaced with croplands, while all other model configurations and forcing remained identical to the control simulation (CTRL).

To quantify the differences in the CUHII of downstream cities in the sensitivity experiments, $\Delta CUHII$ was calculated:

$$\Delta CUHII_i(t) = CUHII_{i,CTRL}(t) - CUHII_{i,EXP}(t), \quad (4)$$

where $CUHII_{i,CTRL}(t)$ and $CUHII_{i,EXP}(t)$ denote the CUHII values in region i derived from the control simulation and the sensitivity experiment, respectively. The criteria for demarcating the rural reference area in the model are given in supplementary material Text S1. A positive $\Delta CUHII$ indicates an increase in the CUHII in downstream cities, and vice versa.

https://doi.org/10.5194/egusphere-2026-1707
Preprint. Discussion started: 14 April 2026

2.2.4 Calculation of BUHI intensity

Thanks to the high spatial resolution of numerical simulations, the BUHII can be further calculated. BUHII is defined as the mean potential temperature difference within the PBL between urban and reference rural areas, and its calculation formula is as follows:

$$BUHII_i(t) = \langle\theta_i\rangle_{\mathrm{PBL}} - \langle\theta_{\mathrm{r}}\rangle_{\mathrm{PBL}}, \quad (5)$$

where $\langle\theta_i\rangle_{\mathrm{PBL}}$ and $\langle\theta_{\mathrm{r}}\rangle_{\mathrm{PBL}}$ represent the mean potential temperature within the boundary layer over urban and rural areas, respectively. Taking the urban area as an example:

$$\langle\theta_i\rangle_{\mathrm{PBL}} = \frac{1}{N_i}\sum_{j=1}^{N_i}\left(\frac{1}{K_{i,j}}\sum_{k=1}^{K_{i,j}}\theta_{i,j,k}(t)\right), \quad (6)$$

where, N_i is the number of grid points in the urban region i; for a given grid point j, $K_{i,j}$ denotes the number of vertical layers from the lowest model level to the PBLH (output by the model); and $\theta_{i,j,k}(t)$ is the potential temperature at time t at the k-th layer of grid point j. The calculation method for the rural area $\langle\theta_{\mathrm{r}}\rangle_{\mathrm{PBL}}$ is similar:

$$\langle\theta_{\mathrm{r}}\rangle_{\mathrm{PBL}} = \frac{1}{N_{\mathrm{r}}}\sum_{j=1}^{N_{\mathrm{r}}}\left(\frac{1}{K_{\mathrm{r},j}}\sum_{k=1}^{K_{\mathrm{r},j}}\theta_{\mathrm{r},j,k}(t)\right), \quad (7)$$

where N_{r} is the number of grid points in the rural area r. Similarly, $\Delta BUHII$ is employed to quantify the difference in BUHII of downstream cities between the control simulation and sensitivity experiments:

$$\Delta BUHII_i(t) = BUHII_{i,CTRL}(t) - BUHII_{i,EXP}(t), \quad (8)$$

where the subscripts CTRL and EXP denote the control simulation and the sensitivity simulation, respectively.

3 Results

3.1 Spatiotemporal characteristics of UHA under prevailing wind conditions

Wind conditions play an important role in modulating the intensity and spatial heterogeneity of the UHI (He, 2018; Yang et al., 2023). The regional background wind speed and direction were derived from four representative observation stations (Fig. 3). The prevailing wind directions exhibit pronounced seasonal variation, which is partly governed by the East Asian monsoon system. During summer (June–August), southeast flows prevail under the influence of the Western Pacific subtropical high (Shi et al., 2025; Zong et al., 2021). Conversely, the frequency of northwest winds increases relatively in winter (December–February), driven by the continental Siberian high (Dai et al., 2025). Spring and autumn serve as transition periods, displaying greater variability in wind direction, and may be influenced by local circulations (e.g., sea breezes and lake breezes) under weak synoptic conditions (Yang et al., 2023). It is noteworthy that the prevailing monsoon direction aligns with the

https://doi.org/10.5194/egusphere-2026-1707
Preprint. Discussion started: 14 April 2026

arrangement of the urban agglomerations, both being northwest-southeast (e.g., the urban U1-U2-U4-U6-U9 and U3-U5-U7), and there are no strong heat sources in the upstream or downstream of rural areas along this direction (Fig. 1b). Therefore, the characteristics of UHA under northwest and southeast wind conditions are discussed in detail.

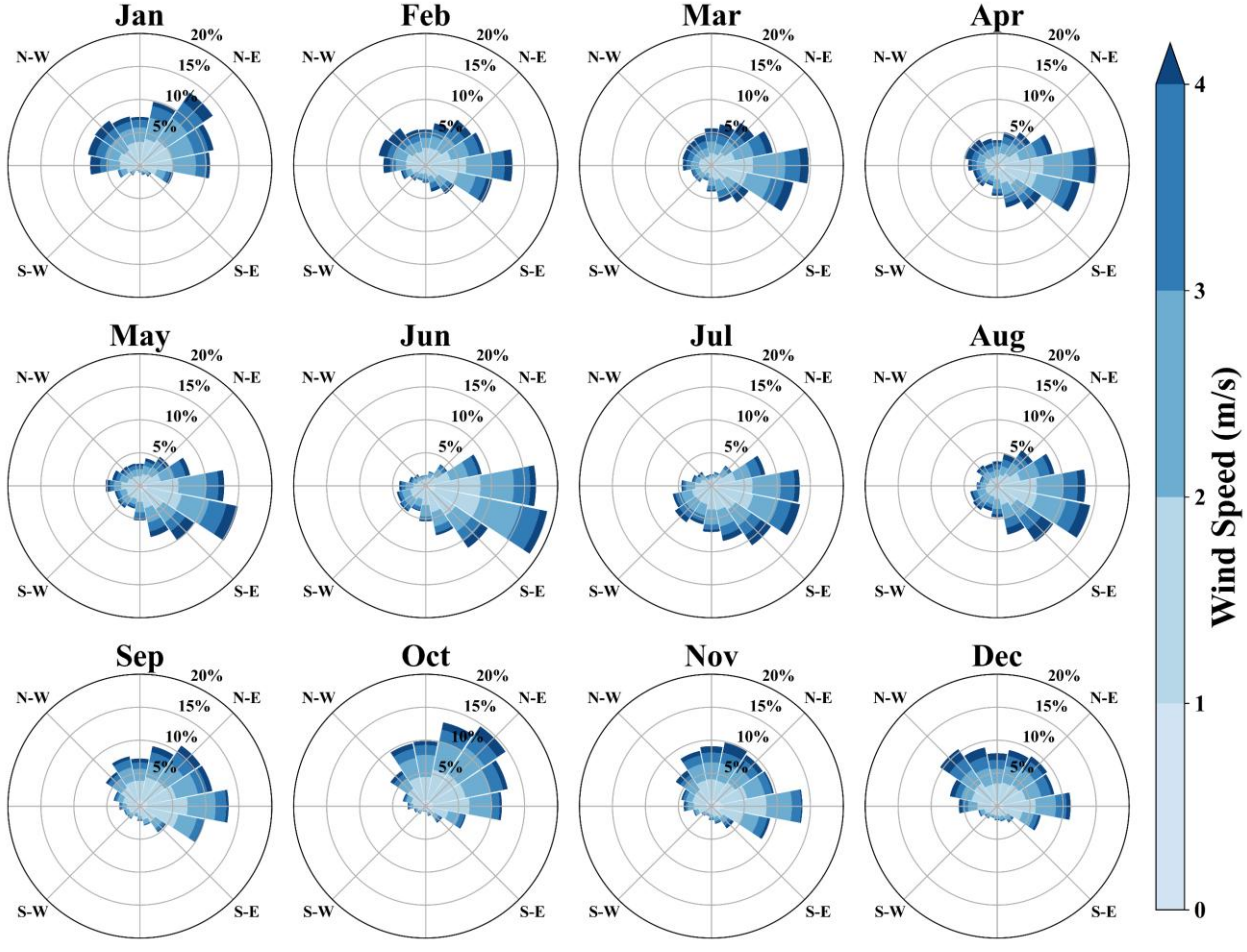

Figure 3. Monthly 10-meter wind rose diagrams based on hourly wind data at four national meteorological stations.

The spatiotemporal characteristics of CUHI and UHA under northwest wind conditions are shown in Supplementary Figure S1 and Figure 4. The regionally daily-averaged CUHII ranges from 0.22°C to 1.38°C and generally shows higher intensity at night than during daytime (Fig. S1). For upstream areas, the daily-averaged UHA intensity is negative (e.g., –0.17°C in region U1, Fig. 4), indicating a mitigation of the CUHI (e.g., U1 exhibits a daytime urban cold island effect, Fig. S1a). Favourable ventilation conditions help reduce the UHI (Zheng et al., 2022), and increasing wind speed usually leads to a decrease in CUHII (Tian et al., 2023). When the wind speed exceeds a critical threshold, the UHI intensity may approach zero (He, 2018). Along the downwind direction, regional UHA intensity changes from negative to positive and progressively strengthens, reaching up to 0.32°C in the strongest downstream region (Fig. 4). This corresponds to daily-mean UHA, while nocturnal peak

https://doi.org/10.5194/egusphere-2026-1707
Preprint. Discussion started: 14 April 2026

values approach 0.6 °C in some regions. This spatial gradient indicates that heat from multiple urban sources is transported and superposed downstream through advection. In addition, UHA exhibits a distinct diurnal contrast, being generally greater at night than during the day, with the average intensity reaching approximately 0.6°C during peak hours in some regions. For regions with positive daily-average UHA intensity (red lines in Fig. 4), the mean nocturnal UHA intensity (~0.4°C) is 319% higher than its daytime counterpart (~0.1°C). In summary, under northwest wind conditions, the regional UHA pattern indicates that upstream areas benefit from ventilation-induced CUHI relief, whereas downstream urban zones experience enhanced heat loading, and UHA intensity shows day–night asymmetry.

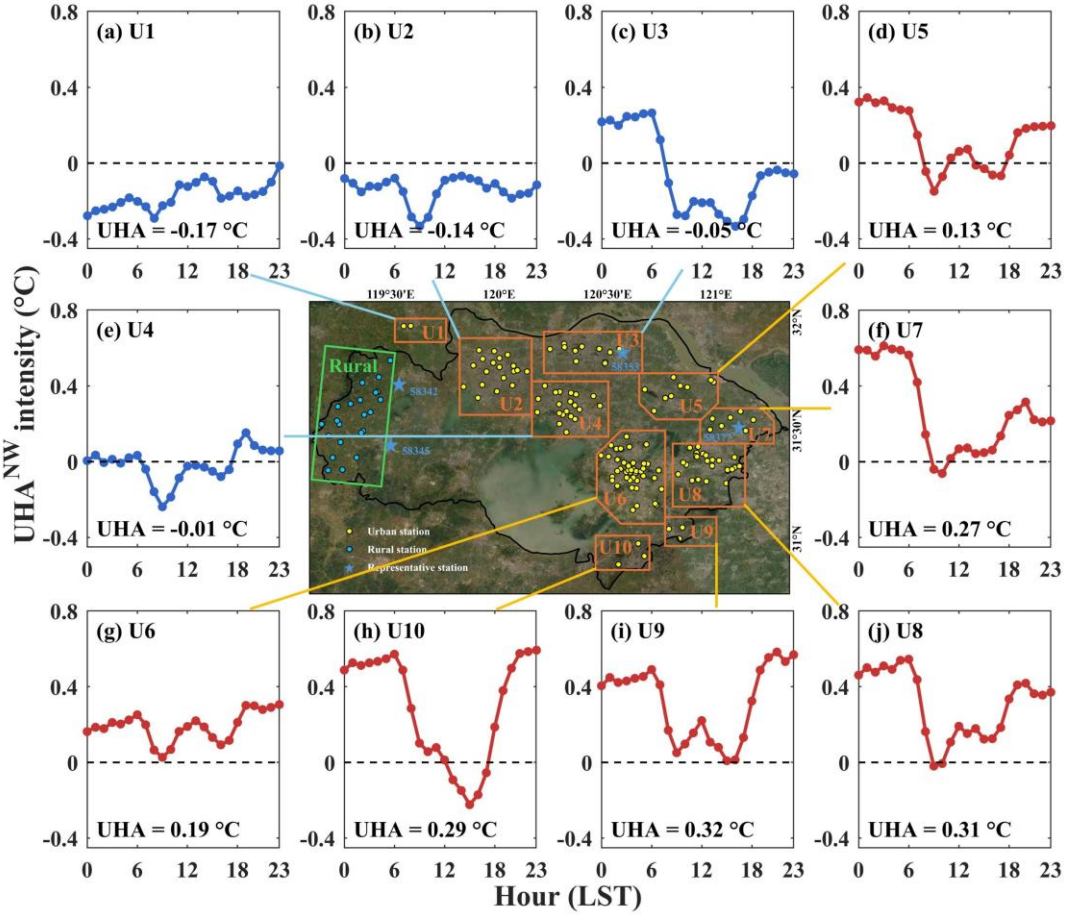

Figure 4. Diurnal variation of hourly UHA intensity across different regions under northwest wind conditions. The numerical values indicate the daily-averaged UHA intensity for each region. Line colours represent the sign of the daily-averaged UHA intensity: red indicates positive values, while blue indicates negative values.

https://doi.org/10.5194/egusphere-2026-1707
Preprint. Discussion started: 14 April 2026

The spatiotemporal characteristics of UHA under southeast and northwest wind conditions exhibit both commonalities and differences. Under southeast wind conditions, a pronounced cooling effect is observed in the upwind region, where the minimum averaged UHA intensity reaches –0.8°C. Similarly, a distinct spatial gradient exists along the prevailing wind vector, characterized by a progressive increase in UHA toward the downwind region, with the maximum daily-averaged intensity reaching 0.09°C (Fig. 5). Regions exhibiting a positive daily-averaged UHA (U1–U3) also demonstrate diurnal asymmetry: the mean nocturnal UHA is approximately 0.15°C, whereas the daytime intensity decreases to –0.05°C. Notably, CUHII also presents a pattern of higher values at nighttime and lower values during daytime (Fig. S2), consistent with the diurnal variation trend of the UHA (red lines in Fig. 4-5), suggesting that the specific contribution of UHA to the urban thermal environment is frequently obscured in conventional CUHI analysis. Overall, although both wind directions facilitate upwind ventilation and downwind heat accumulation, their net thermal effects differ. Northwest winds mainly exacerbate the CUHI across most regions of the study area, whereas southeast winds exert a more extensive mitigating influence. Consequently, the subsequent sections investigate the driving factors of UHA specifically under northwest wind conditions.

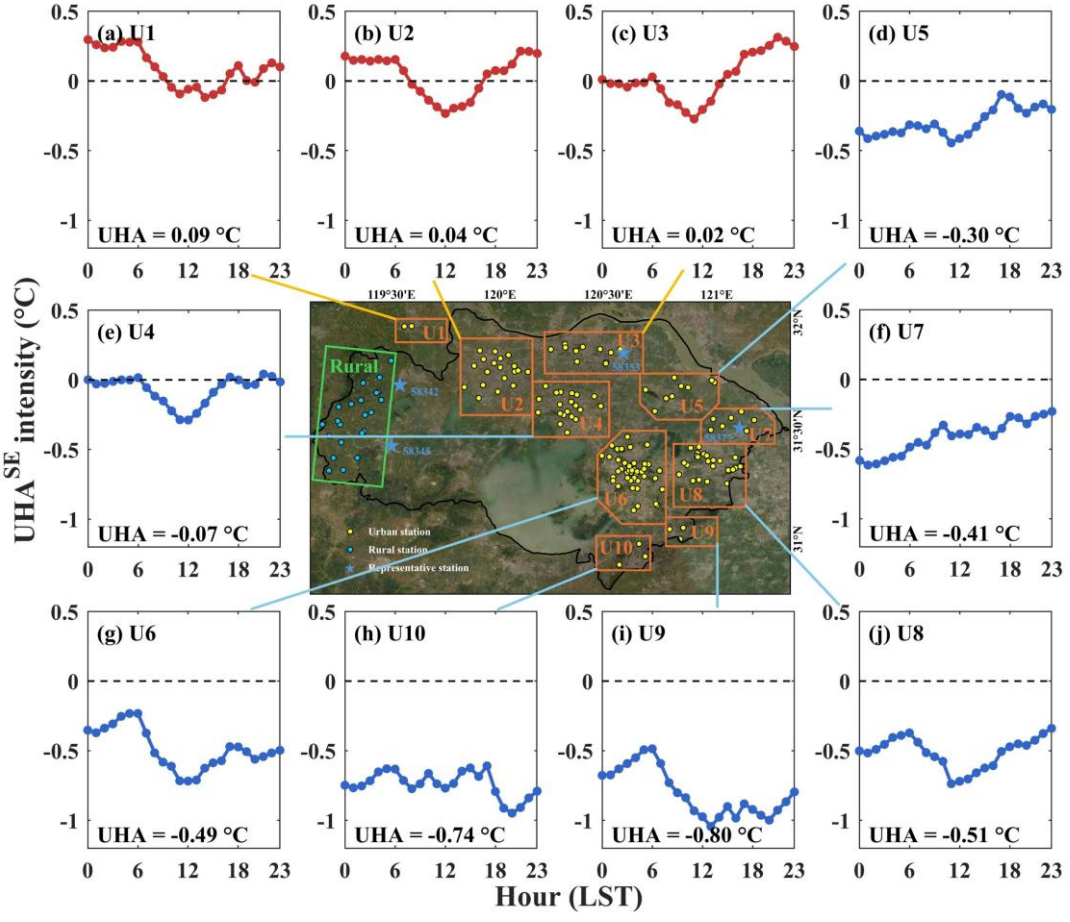

Figure 5. Same as Figure 4, but under southeast wind conditions.

https://doi.org/10.5194/egusphere-2026-1707
Preprint. Discussion started: 14 April 2026

3.2 Changes in UHA with wind speed and PBLH

UHA intensity is modulated by meteorological conditions. Previous studies have discussed nocturnal UHA in some cities, such as Birmingham (temperate maritime climate) (Bassett et al., 2016) and Lubbock (semi-arid climate) (Danzig et al., 2025), finding that wind speed and direction are important factors influencing UHA. Extending beyond prior nocturnal analyses, this study examines UHA under both daytime and nighttime conditions while incorporating PBLH as an additional parameter. Daytime (typically characterized by unstable boundary layer conditions) was defined as 08:00–19:00 local time, while nighttime (typically characterized by stable boundary layer conditions) spans 20:00–07:00 (Zhang et al., 2023). Screening was conducted according to the following criteria: mean 10-meter wind speed < 4 m s^{-1} and mean PBLH < 1400 m (700 m) for daytime (nighttime) conditions, with 93.13% (94.48%) of the samples meeting the requirements. This section discusses the relationships between UHA intensity, wind field, and PBLH under nocturnal and diurnal conditions.

In a stable boundary layer, the advection term often dominates the surface heat budget (Stull, 1988). Figure 6 presents the nocturnal UHA intensity as a function of wind speed and PBLH across different regions. For the downstream region with a positive mean UHA (red line in Fig. 6), UHA intensity generally increases and then decreases with increasing wind speed and PBLH. Statistical analysis indicates a significant positive correlation between nighttime wind speed and PBLH (Fig. S3a), r = 0.79 ($p < 0.001$). The variation in UHA appears closely linked to boundary layer processes. In a very stable boundary layer, characterized by weak winds, low PBLH, intermittent and weak turbulence (Sun et al., 2012; Xue et al., 2025; Zhang et al., 2024b), suppressing horizontal heat transport and vertical mixing. As wind speed and PBLH increase, horizontal advection and turbulence (driven by mechanical shear) strengthen (Mahrt, 2014), and UHA intensity reaches its peak (e.g., in region U7, the mean UHA intensity can reach 0.88°C in the wind speed range of 2–3 m s^{-1}, see Fig. 6g1). This phenomenon is consistent with observations in Birmingham and Lubbock (Bassett et al., 2016; Danzig et al., 2025). Consequently, the peak impact of nocturnal UHA typically occurs under moderate wind speed conditions, and this pattern may be universal across cities with different climatic backgrounds. When wind speed further increases, and the stable boundary layer transitions to a neutral boundary layer, vertical turbulent exchange intensifies, promoting vertical dilution of urban heat, leading to a decrease in UHA, which may even produce negative values in some regions (e.g., U3–U6; Fig. 6c–f). Furthermore, for upstream regions with negative mean UHA (e.g., U1), UHA intensity decreases with increasing wind speed and PBLH, demonstrating the mitigating effect of ventilation on CUHI. In summary, nocturnal UHA intensity is nonlinearly modulated by wind speed and boundary layer turbulence, with maximum UHA typically occurring under moderate wind and PBLH conditions.

https://doi.org/10.5194/egusphere-2026-1707
Preprint. Discussion started: 14 April 2026

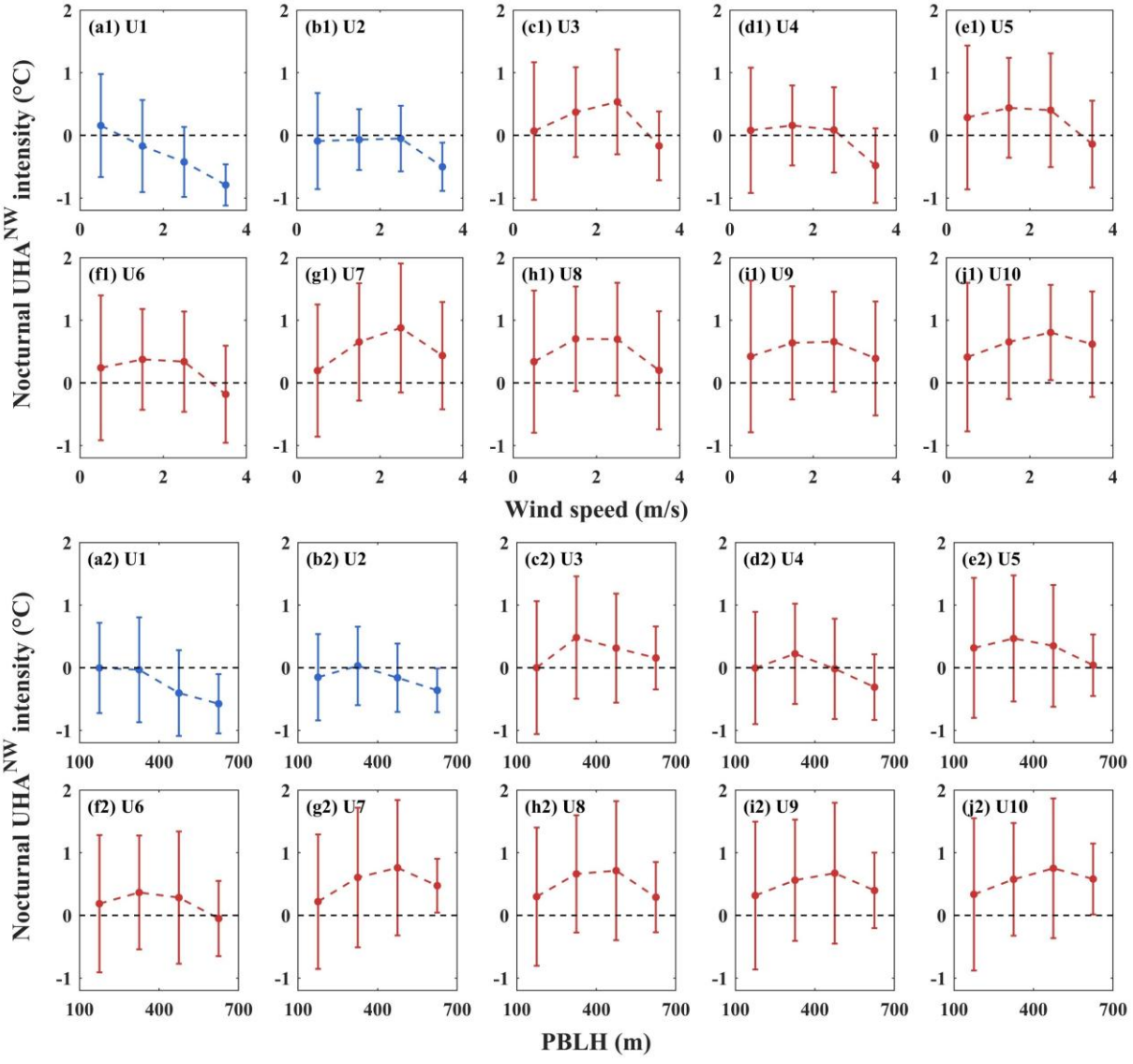

Figure 6. Nocturnal averaged UHA intensity as functions of (a1-j1) wind speed and (a2-j2) PBLH across different regions. Line colours represent the sign of the nocturnal averaged UHA intensity: red indicates positive values, while blue indicates negative values. The bars indicate the standard deviation.

Advection partially contributes to the thermal budget of the convective boundary layer (Stull, 1988). Figure 7 illustrates the daytime variation in UHA intensity as a function of wind speed and PBLH. In downwind regions characterized by a positive daytime mean UHA (red lines in Fig. 7), no systematic correlation is observed between wind speed and UHA intensity; overall, UHA intensity was relatively higher under low wind speed conditions. In contrast, UHA exhibits a pronounced negative dependence on PBLH. As PBLH increased, daytime UHA intensity decreased significantly. When PBLH exceeds 800 m, the

https://doi.org/10.5194/egusphere-2026-1707
Preprint. Discussion started: 14 April 2026

mean UHA intensity shifts to negative values across all regions, with the lowest intensity at approximately -0.6°C. In daytime convective boundary layers, intense buoyancy-generated turbulence deepens the PBL (Xian et al., 2024) and efficiently redistributes urban heat, which suppresses downstream canopy-level UHA and can even lead to a net cooling relative to upwind conditions.. Although a positive correlation between daytime wind speed and PBLH persists (Fig. S3b, $r = 0.5$, $p < 0.001$), this positive correlation weakens relative to nocturnal conditions. Therefore, thermally driven turbulent mixing acts as a critical moderating factor for daytime UHA intensity, with peak UHA intensity typically manifesting under low PBLH conditions.

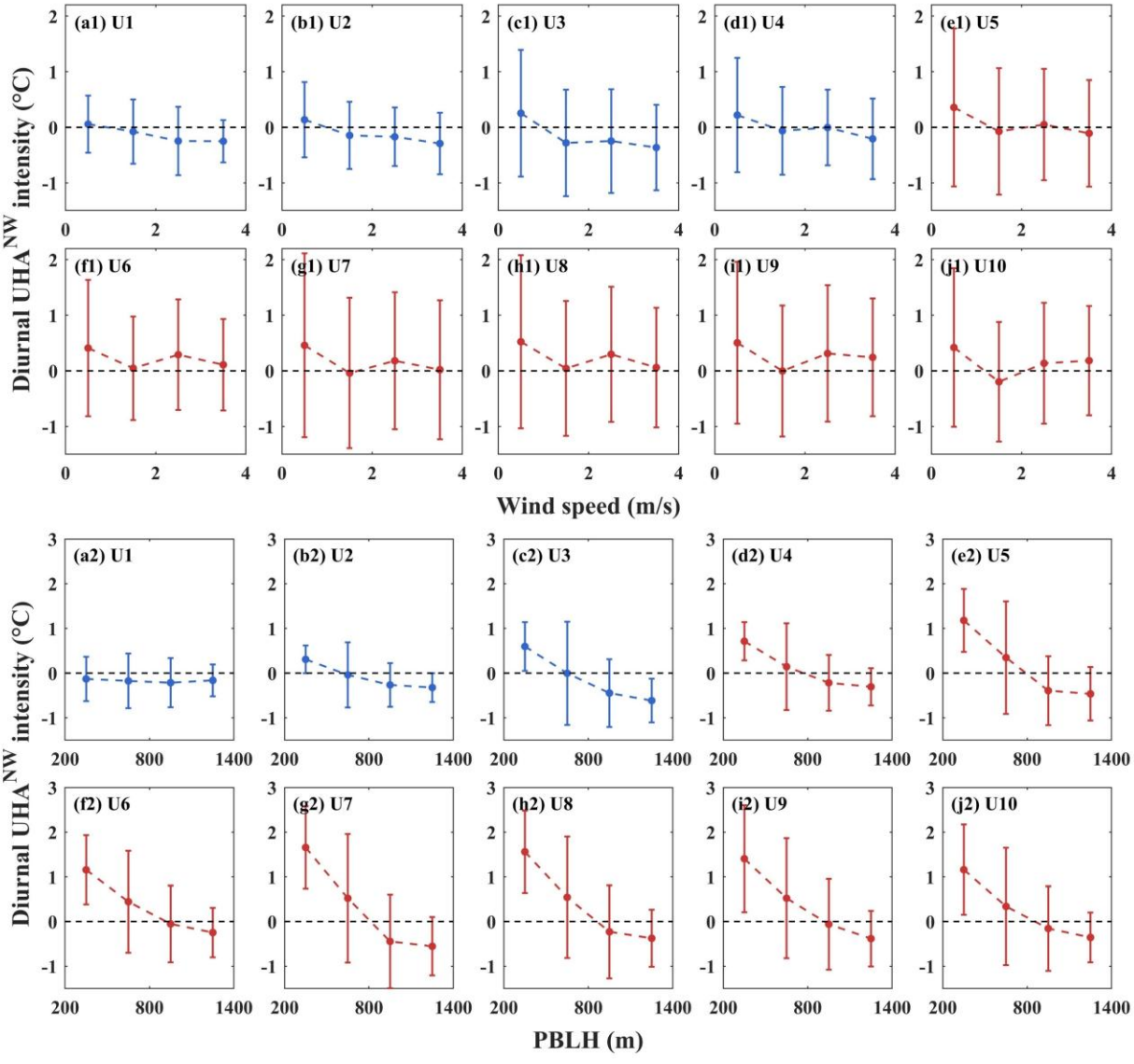

Figure 7. Same as Figure 6, but under diurnal conditions.

https://doi.org/10.5194/egusphere-2026-1707
Preprint. Discussion started: 14 April 2026

3.3 Sensitivity analysis of UHA using the WRF numerical model

Numerical simulations were employed to investigate UHA characteristics at higher spatial resolution. Sensitivity experiments utilizing modified LULC configurations have become a mature approach for quantifying urban impacts on regional thermal environments (Moustaoui and Georgescu, 2025; Zhao et al., 2021). In the sensitivity experiment, the LULC within the downtown area of Changzhou (U2) was replaced with croplands to isolate approximately the thermal contribution of urbanization to downstream regions (methodology detailed in Sect. 2.2.3), particularly the impact on the downtown areas of Wuxi (U4) and Suzhou (U6). Model performance was evaluated by comparing simulated 2-m air temperature of domain 3 against hourly observations from all available meteorological stations within the ROI (Fig. 8). The results show that the root mean square error (RMSE) and coefficient of determination (R^2) were 1.44°C and 0.84 ($p < 0.001$), respectively, demonstrating that the WRF model reasonably reproduced observed thermal environment.

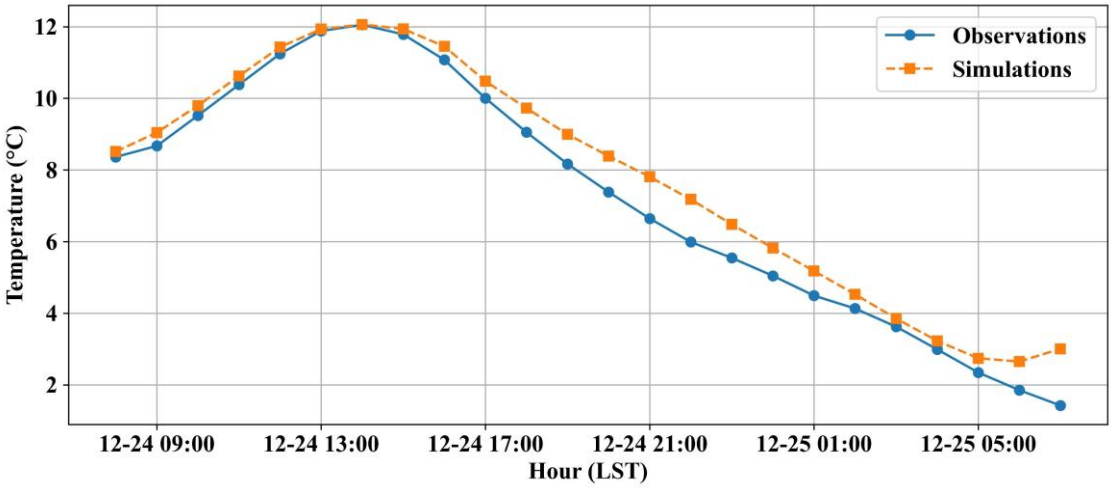

Figure 8. Comparison of hourly mean 2-meter temperature from WRF simulations and observations within the ROI.

Figure 9 illustrates the spatial distribution of the 2-meter temperature difference between the control and sensitivity simulations (CTRL minus EXP), approximately representing the thermal contribution of upstream urbanization in Changzhou to the downstream canopy temperature. During the analysis hours, northwest winds prevailed in domain 3. Influenced by the UHI, Changzhou exhibited a pronounced warming, with positive temperature anomalies of 2.43 °C and 0.19 °C at 23:00 BST and 12:00 BST, respectively. The simulations show a diurnal variation in the 2-meter temperature differences. At night (23:00 BST), lower wind speeds accompanied by a high UHA intensity but with a limited advective distance, and strong warming was concentrated in the short distance downstream of the city (Fig. 9a). In contrast, daytime conditions (12:00 BST) featured higher wind speeds, which accompanied by lower UHA intensity but a greater thermal influence distance (Fig. 9b). Under the prevailing northwest winds, the U10 region was also affected by the thermal forcing of Taihu Lake in addition to UHA. During winter, Taihu Lake functions as a daytime heat sink and a nighttime heat source relative to the surrounding environment (Fig.

https://doi.org/10.5194/egusphere-2026-1707
Preprint. Discussion started: 14 April 2026

S4). Furthermore, Cosgrove and Berkelhammer (2018) utilized a Lagrangian atmospheric transport model to demonstrate that the Chicago urban thermal plume caused significant heating at 100–200 m above ground level, extending up to 70 km downwind. The sensitivity experiments in this study show that the downstream canopy region was also heated, with the thermal influence beyond 100 km.

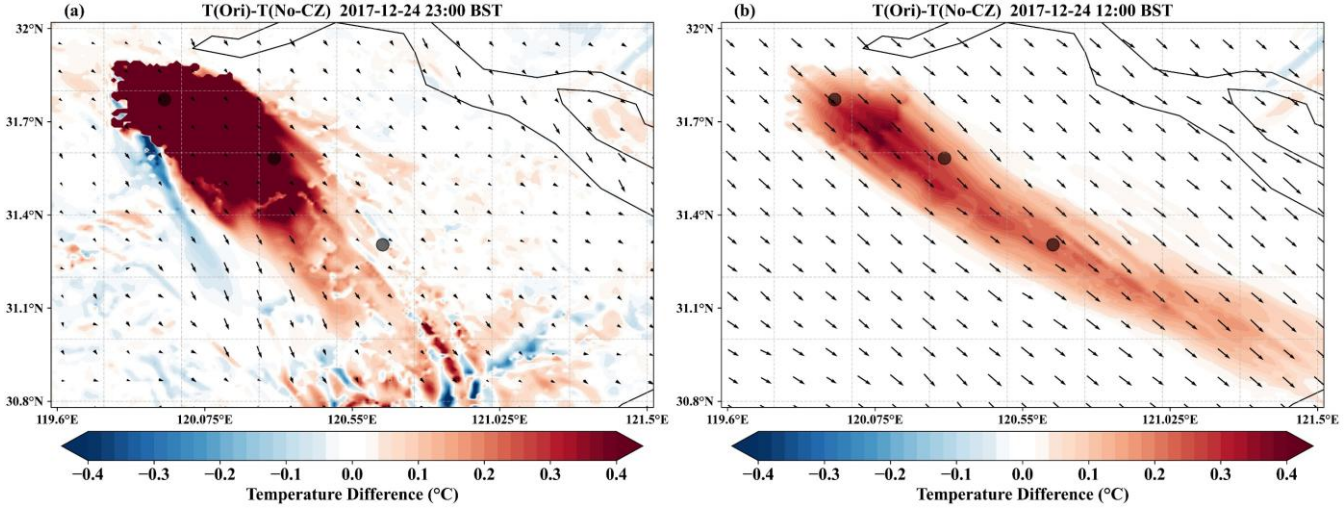

Figure 9. Spatial distribution of the 2-meter temperature difference between the control simulation and the sensitivity experiment (CTRL minus EXP) at (a) 23:00 BST and (b) 12:00 BST. Vector arrows indicate the 10-meter wind field of the CTRL. The three marked locations from northwest to southeast correspond to downtown areas of Changzhou (U2), Wuxi (U4), and Suzhou (U6), respectively.

Vertical cross-sections of potential temperature and wind vector differences between control and sensitivity experiments were analysed (Fig. 10). The cross-section along a northwest-southeast direction spans approximately 114 km (Fig. 10a), encompassing cities from Changzhou (U2) through Wuxi (U4) to Suzhou (U6). Note that the coordinate rotation was applied to the horizontal wind component u to align it with the cross-section direction, with positive values corresponding to northwest winds. For example, significant negative horizontal wind components within Changzhou's near-surface layer are due to the urban rough surface. At night (23:00 BST), the atmospheric stratification is stable, and updrafts and downdrafts induced by the UHI can be observed over urban areas, particularly in Wuxi (see the CTRL results in Figure S5b). Thermal plume was suppressed within the near-surface layer, and substantial heat within the Changzhou propagated downstream primarily below 80 m, although the PBLH can reach 300-750 m (Fig. 10b). Following sunrise, solar shortwave radiation enhanced surface heating and buoyancy-driven turbulence (Zhang et al., 2023), elevating PBLH to approximately 1200 m by noon (12:00 BST, Fig. S5c). Compared to nighttime conditions, enhanced ventilation and vertical mixing extended thermal influences throughout the entire PBL depth (Fig. 10c), intensifying the BUHI in Wuxi and Suzhou. As the thermal plume propagates, vertical heat

https://doi.org/10.5194/egusphere-2026-1707
Preprint. Discussion started: 14 April 2026

redistribution may occur through turbulent mixing in downstream cities. In addition, the updraft in the downstream area is strengthened, and the vertical circulation in Wuxi during the day may be UHA-enhanced UHI circulation (Fig. 10b-c).

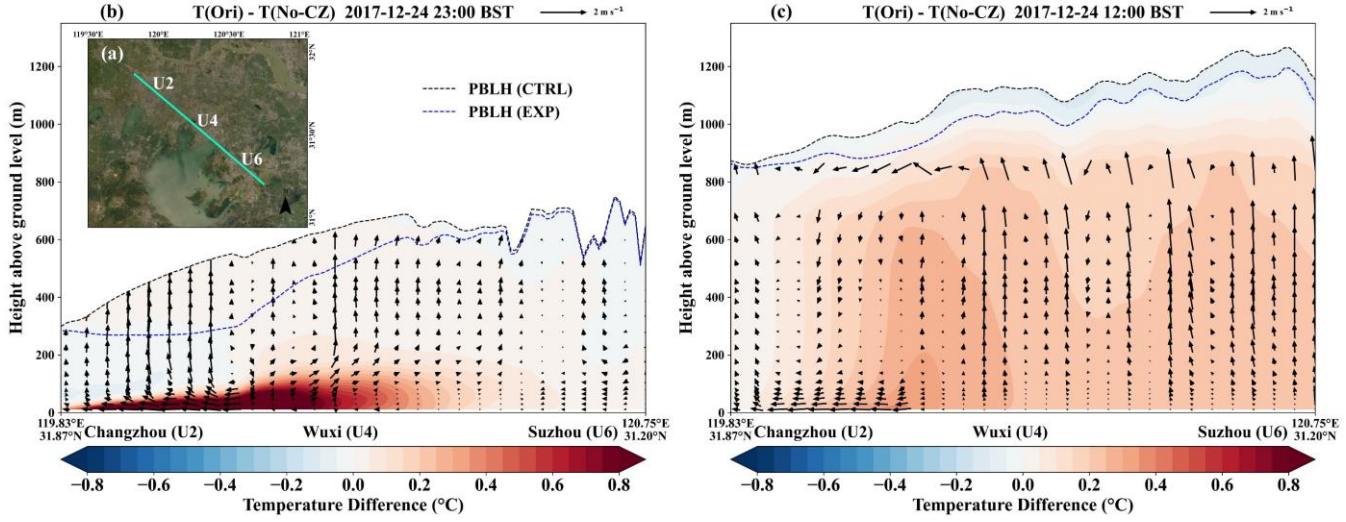

Figure 10. (a) Geographical location of the vertical cross-section. (b, c) Vertical cross-sections of the potential temperature and wind vector differences between the control simulation and the sensitivity experiment (CTRL minus EXP) at (b) 23:00 BST and (c) 12:00 BST. Wind vectors were synthesized by rotating u (along the transect axis) and scaling ω (ω multiplied by 50). The black and blue solid lines denote the PBLH in the CTRL and EXP simulations, respectively.

The sensitivity experiments quantified UHA contributions from a single upstream city. In reality, taking the downstream city of Suzhou as an example, its UHI is influenced by multiple upstream heat sources, including weak UHA transport from distant Changzhou superimposed upon strong UHA contributions from adjacent Wuxi. If the LULCs in upstream Changzhou and Wuxi are simultaneously replaced with croplands in the sensitivity experiment, enhanced cross-city thermal plume superposition and greater PBLH differences were shown (Fig. S6). These results demonstrate that the intensity and spatial structure of UHA are closely related to diurnal boundary layer evolution.

The CUHII differences of the downstream adjacent city Wuxi (U4) were evaluated between two experimental scenarios. Figures 11a–d show scatter plots of ΔCUHII and both wind speed and PBLH across different hours. Nighttime conditions exhibited a higher ΔCUHII (with a maximum increase of 0.59°C), accompanied by lower wind speed and shallower PBLH (Fig. 11a1–a2); while daytime conditions showed a comparatively lower ΔCUHII (with a minimum increase of 0.12°C), accompanied by higher wind speed and deeper PBLH (Fig. 11a3–a4). The relative increase in CUHII ranged from 9.1% to 42.2%, with the large proportional amplifications occurring during the nocturnal period. ΔBUHII ranges from about 0.12 to 0.35 °C (19.2–141.2%), indicating a larger relative sensitivity of the boundary-layer UHI to upstream UHA than at canopy level. At night, ΔCUHII exhibited a non-linear response to increases in wind speed and PBLH, characterized by an initial amplification followed by a decrease (Fig. 11a1–a2). In contrast, daytime ΔCUHII decreased with increasing PBLH, while its

https://doi.org/10.5194/egusphere-2026-1707
Preprint. Discussion started: 14 April 2026

correlation with wind speed remained ambiguous (Fig. 11a3–a4). Wind speed and PBLH exhibited a strong positive correlation at night ($p < 0.001$, Fig. S7a), but no statistical significance during the day ($p = 0.36$, Fig. S7b). While the WRF-SLUCM typically overestimates 10m wind speed (Avisar et al., 2021) and PBLH (Silva et al., 2021), this bias does not compromise the qualitative assessment of ΔCUHII variation in response to these meteorological parameters. Furthermore, the enhancement of downstream CUHII (i.e., ΔCUHII) is primarily contributed to by UHA, though it is not entirely attributable to this mechanism; it is concurrently modulated by other physical processes. For example, advective transport from upstream urban areas can modify local atmospheric conditions (e.g., ambient humidity, stability), which subsequently influence the thermal environment of the downstream city. In summary, these sensitivity experiments provide corroborations for the observational findings, confirming that UHA is regulated by wind speed and PBLH non-linearly.

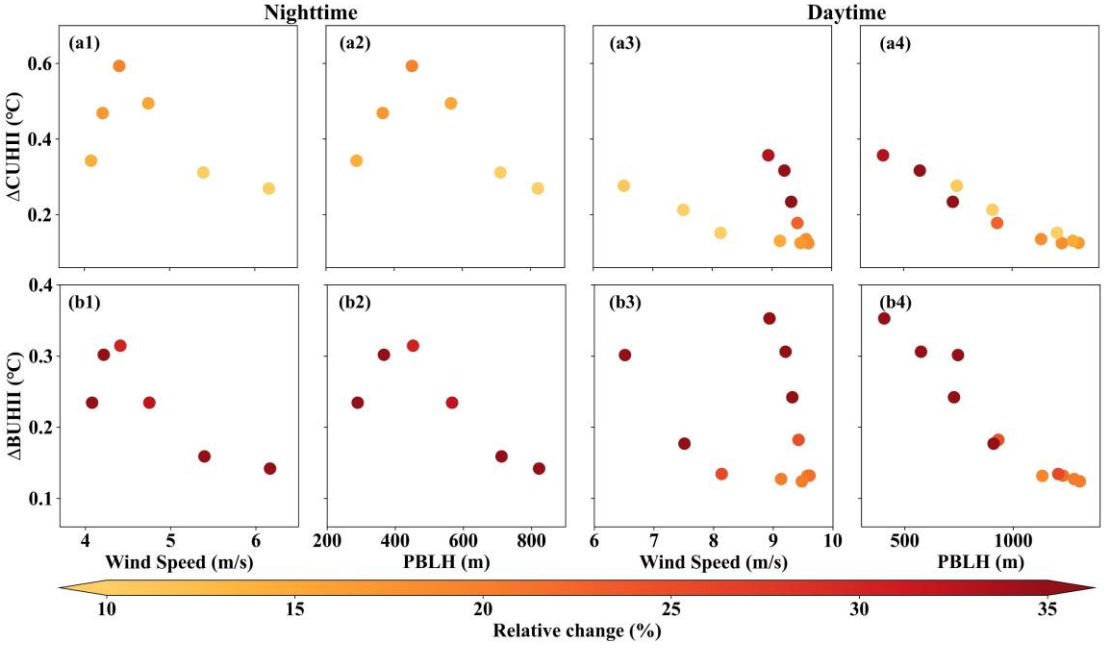

Figure 11. Scatter plots between ΔCUHII and (a1, a3) 10-meter wind speed, and (a2, a4) PBLH between the control simulation and the sensitivity experiment (CTRL minus EXP) at (a1-a2) nighttime and (a3-a4) daytime. (b1-b4) Same as (a1-a4), but for ΔBUHII. Colours represent the relative change of CUHII or BUHII. Note that only the moment when the northwest wind prevailed in the ROI was reserved.

UHA also contributed to an increase in BUHII in the downstream city of Wuxi (U4, Fig. 11b1–b4). Specifically, ΔBUHII increased by a maximum of 0.35°C and a minimum of 0.12°C, ranging from 19.2% to 141.2%. Compared to ΔCUHII, the relative percentage change range of ΔBUHII was larger. In addition, because the numerical simulation covered a limited time period, the potential moderating roles of wind speed and PBLH on BUHI were not further examined.

https://doi.org/10.5194/egusphere-2026-1707
Preprint. Discussion started: 14 April 2026

4 Discussions

In the context of climate change and rapid urbanization, urban impacts on regional climate are increasingly significant. At local to regional scales, these thermal impacts can rival or exceed the greenhouse effect (Cosgrove and Berkelhammer, 2018), intensifying cooling energy demand in summer (Fung et al., 2006) while mitigating heating requirements in winter (Meng et al., 2020). Our results extend previous UHA studies focused on isolated cities by quantifying cross-city superposition of urban heat plumes within a large urban agglomeration and by demonstrating the modulation of this process by PBLH using both observations and targeted WRF sensitivity experiments. When background winds are present, UHA propagates heat downstream. Particularly with urban agglomeration development and decreasing inter-city distances, spatial clustering of heat sources amplifies regional thermal risks. Based on observations and numerical simulations, Figure 12 presents a conceptual diagram of UHA impacts on downwind UHI in the YRD urban agglomeration. On the one hand, cities transfer heat downstream within the canopy layer or near-surface layer, particularly during nocturnal stable boundary layer conditions, where UHA impacts are confined to relatively low vertical height (Cosgrove and Berkelhammer, 2018) (orange arrow in Fig. 12). Vertical mixing of shallow PBL and weak turbulence is detrimental to cooling of the built-up area environment (Haeffelin et al., 2024). On the other hand, as urban thermal plumes are transported downstream over long distances within the PBL, they can be vertically mixed with the lower-level air of downstream cities through turbulence (above the downstream city in Fig. 12). During daytime convective boundary layer conditions, buoyancy-driven turbulence is vigorous, and the vertical thermal impact of the UHA can extend throughout the entire PBL depth. Consequently, thermal plumes from successive cities coalesce and facilitate further heat transport (Fig. 12). However, this study only quantified UHA impacts on CUHII and BUHII in downstream cities, without partitioning contributions from horizontal canopy transport and vertical mixing processes of thermal plume. Additionally, downstream cities receive not only heat but also aerosol inputs from upwind urban sources (Baklanov et al., 2016). These aerosols may modulate the CUHII of downstream cities through radiative forcing (Wang et al., 2020; Xue et al., 2023; Yang et al., 2020), and this feedback process warrants further investigation.

https://doi.org/10.5194/egusphere-2026-1707
Preprint. Discussion started: 14 April 2026

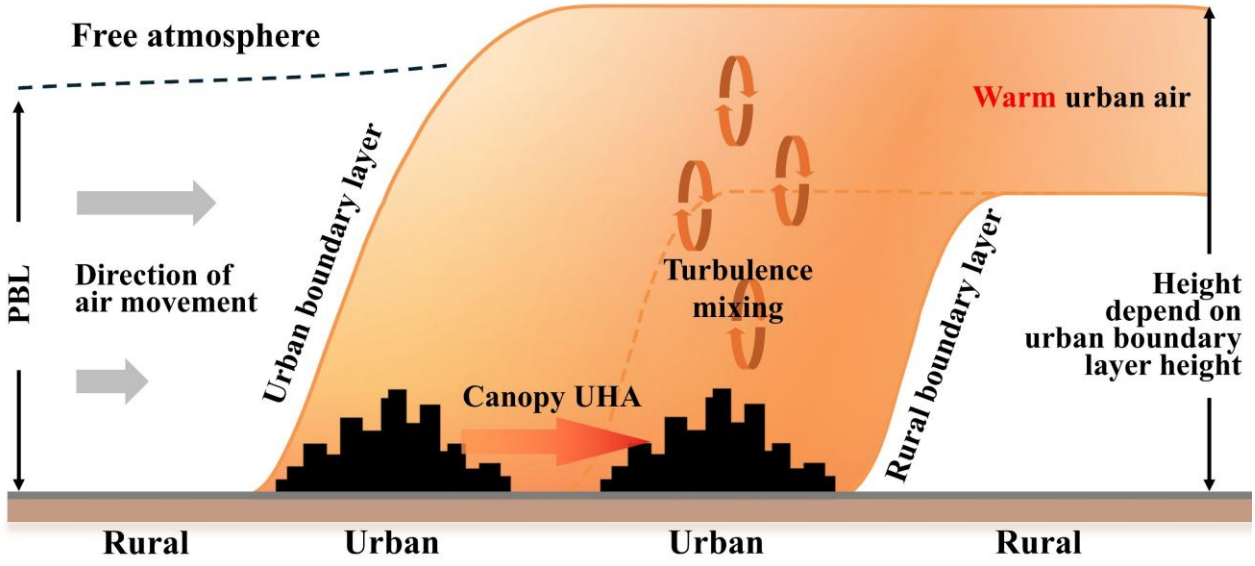

385 **Figure 12.** Conceptual diagram showing the impact of UHA on downstream urban UHI within the Yangtze River Delta urban agglomeration. Modified from Oke (1976) and Cosgrove and Berkelhammer (2018).

5 Conclusions

In this study, we combined five years of high-density automatic weather station observations with WRF-SLUCM simulations to quantify how urban heat advection (UHA) links urban heat islands (UHIs) across the Suzhou–Wuxi–Changzhou
390 metropolitan area in the Yangtze River Delta (YRD), China. Our results demonstrate that UHA exhibits pronounced spatiotemporal variability and systematically transports heat from upwind to downwind cities along the prevailing monsoon-related wind directions. Under north-westerly flow, daily-mean UHA intensity changes from negative values in upwind regions to about 0.3 °C in the most affected downstream areas, with nocturnal UHA during peak hours reaching roughly 0.6 °C and exceeding daytime values by a factor of three.

395 We show that UHA is non-linearly modulated by wind speed and planetary boundary-layer height (PBLH). At night, when the boundary layer is shallow and stable, maximum downstream warming occurs under moderate wind speeds and intermediate PBLH, consistent with an advection-dominated regime. In contrast, deep daytime convective boundary layers (PBLH ≥ 800 m) efficiently dilute urban heat plumes, suppressing downstream canopy-layer UHA and in some cases producing a net cooling relative to upwind conditions. These findings highlight the central role of boundary-layer dynamics in regulating the magnitude
400 and sign of UHA within urban agglomerations.

Targeted WRF land-use sensitivity experiments further reveal that upstream urbanization substantially enhances downstream UHI intensity. Urban land cover in Changzhou increases CUHII in the adjacent downstream city of Wuxi by up to about 0.6 °C (9–42%) and BUHII by up to about 0.35 °C (19–141%), with detectable canopy-level warming extending beyond 100 km

https://doi.org/10.5194/egusphere-2026-1707
Preprint. Discussion started: 14 April 2026

downwind. Compared with CUHII, BUHII exhibits larger relative changes, indicating a high sensitivity of the boundary-layer UHI to upstream thermal forcing. Taken together, the observations and simulations provide quantitative evidence that cross-city superposition of UHAs is a key physical process coupling UHIs within large urban agglomerations.

These results have several implications for regional climate assessment and heat-risk management. First, neglecting UHA can lead to systematic underestimation of heat exposure in downwind cities, particularly during nocturnal stable conditions. Second, because UHA is strongly constrained by wind direction and PBLH, the realistic representation of boundary-layer processes is essential in regional climate and air-quality models over urban agglomerations. Third, heat-mitigation strategies should consider cross-city coordination along prevailing wind corridors, as local interventions in upwind cities can propagate benefits (or disbenefits) far downstream. Future work should extend the present analysis to other seasons and synoptic regimes, explore compound UHA–pollution events, and assess how projected changes in urbanization and boundary-layer structure may alter the spatial extent and intensity of UHA in rapidly developing urban regions.

Data availability statement

The hourly automated weather stations observation data are available upon request from the China Meteorological Data Service Center (http://data.cma.cn/en, last access: 17 March 2026). The anthropogenic heat flux data are available at https://doi.org/10.7910/DVN/VIJFPK (Qian et al., 2024). The built-up area data are accessed at http://irsip.whu.edu.cn/resv2/dataweb.php# (Huang et al., 2021). The planetary boundary layer height data are available at https://doi.org/10.5281/zenodo.6498004 (Guo et al., 2024). Final Operational Global Analysis (FNL) data were derived from the National Centers for Environmental Prediction at https://doi.org/10.5065/D65Q4T4Z. The MODIS land cover product (MCD12Q1, Version 6.1) is available at https://doi.org/10.5067/MODIS/MCD12Q1.061 (Friedl and Sulla-Menashe, 2022).

Author contributions

YY conceptualized the study and designed the experiments. JX wrote the original manuscript and plotted all the figures. JX, GR, and SL assisted in the conceptualization and model development. All the authors contributed to the manuscript preparation, discussion, and writing.

Competing interests

The contact author has declared that none of the authors has any competing interests.

https://doi.org/10.5194/egusphere-2026-1707
Preprint. Discussion started: 14 April 2026

Acknowledgements

We acknowledge the High-Performance Computing Center of Nanjing University of Information Science & Technology for supporting this work. We thank Junfeng Miao, Tao Shi, and Xingxing Ma for valuable comments.

Financial support

This study was supported by the National Natural Science Foundation of China (grant no. 42521006) and the Natural Science Foundation of Jiangsu Province, China (No. BK20250750).

References

Avisar, D., Pelta, R., Chudnovsky, A., and Rostkier-Edelstein, D.: High Resolution WRF Simulations for the Tel-Aviv Metropolitan Area Reveal the Urban Fingerprint in the Sea-Breeze Hodograph, JGR Atmospheres, 126, e2020JD033691, https://doi.org/10.1029/2020JD033691, 2021.

Baklanov, A., Molina, L. T., and Gauss, M.: Megacities, air quality and climate, Atmospheric Environment, 126, 235–249, https://doi.org/10.1016/j.atmosenv.2015.11.059, 2016.

Bassett, R., Cai, X., Chapman, L., Heaviside, C., Thornes, J. E., Muller, C. L., Young, D. T., and Warren, E. L.: Observations of urban heat island advection from a high-density monitoring network, Quart J Royal Meteoro Soc, 142, 2434–2441, https://doi.org/10.1002/qj.2836, 2016.

Bassett, R., Cai, X., Chapman, L., Heaviside, C., and Thornes, J. E.: The Effects of Heat Advection on UK Weather and Climate Observations in the Vicinity of Small Urbanized Areas, Boundary-Layer Meteorol, 165, 181–196, https://doi.org/10.1007/s10546-017-0263-0, 2017.

Bassett, R., Cai, X., Chapman, L., Heaviside, C., and Thornes, J. E.: Semi-idealized urban heat advection simulations using the Weather Research and Forecasting mesoscale model, Intl Journal of Climatology, 39, 1345–1358, https://doi.org/10.1002/joc.5885, 2019.

Brandsma, T., Können, G. P., and Wessels, H. R. A.: Empirical estimation of the effect of urban heat advection on the temperature series of De Bilt (The Netherlands), Intl Journal of Climatology, 23, 829–845, https://doi.org/10.1002/joc.902, 2003.

Brousse, O., Simpson, C., Walker, N., Fenner, D., Meier, F., Taylor, J., and Heaviside, C.: Evidence of horizontal urban heat advection in London using six years of data from a citizen weather station network, Environ. Res. Lett., 17, 044041, https://doi.org/10.1088/1748-9326/ac5c0f, 2022.

Chen, S., Yang, Y., Deng, F., Zhang, Y., Liu, D., Liu, C., and Gao, Z.: A high-resolution monitoring approach of canopy urban heat island using a random forest model and multi-platform observations, Atmos. Meas. Tech., 15, 735–756, https://doi.org/10.5194/amt-15-735-2022, 2022.

Chou, M.-D. and Suarez, M. J.: An efficient thermal infrared radiation parameterization for use in general circulation models, NASA Tech. Memo., 1994.

https://doi.org/10.5194/egusphere-2026-1707
Preprint. Discussion started: 14 April 2026

Cosgrove, A. and Berkelhammer, M.: Downwind footprint of an urban heat island on air and lake temperatures, npj Clim Atmos Sci, 1, 46, https://doi.org/10.1038/s41612-018-0055-3, 2018.

Dai, Y.-L., Sun, B., Zhou, B.-T., Li, H.-X., He, S., Li, F., Huang, Y.-T., and Tang, W.-C.: Intensified extreme cold surges in northern East Asia and the associated changes in atmospheric circulation under climate change, Advances in Climate Change Research, 16, 960–973, https://doi.org/10.1016/j.accre.2025.07.003, 2025.

Danzig, T. B., Pal, S., Medley, Z., Dhaliwal, H., Hamel, M., Sorensen, M., Das, D., Menon, K. V., Lee, T. R., and Conder, M.: Impact of advection on the urban heat of a small-sized city: The Urban Heat island Experiment Around Lubbock, Texas (U-HEAT), Urban Climate, 64, 102714, https://doi.org/10.1016/j.uclim.2025.102714, 2025.

Dinda, A. and Chatterjee, S.: Assessing the local- impacts of heat advection on urban heat islands in Kolkata Metropolitan Area, Urban Climate, 42, 101139, https://doi.org/10.1016/j.uclim.2022.101139, 2022.

Dirks, R. A.: Urban atmosphere: Warm dry envelope over St. Louis, J. Geophys. Res., 79, 3473–3475, https://doi.org/10.1029/JC079i024p03473, 1974.

Friedl, M. and Sulla-Menashe, D.: MODIS/Terra+Aqua Land Cover Type Yearly L3 Global 500m SIN Grid V061, https://doi.org/10.5067/MODIS/MCD12Q1.061, 2022.

Fung, W., Lam, K., Hung, W., Pang, S., and Lee, Y.: Impact of urban temperature on energy consumption of Hong Kong, Energy, 31, 2623–2637, https://doi.org/10.1016/j.energy.2005.12.009, 2006.

Guo, J., Zhang, J., Shao, J., Chen, T., Bai, K., Sun, Y., Li, N., Wu, J., Li, R., Li, J., Guo, Q., Cohen, J. B., Zhai, P., Xu, X., and Hu, F.: A merged continental planetary boundary layer height dataset based on high-resolution radiosonde measurements, ERA5 reanalysis, and GLDAS, Earth Syst. Sci. Data, 16, 1–14, https://doi.org/10.5194/essd-16-1-2024, 2024.

Haeffelin, M., Ribaud, J.-F., Céspedes, J., Dupont, J.-C., Lemonsu, A., Masson, V., Nagel, T., and Kotthaus, S.: Impact of boundary layer stability on urban park cooling effect intensity, Atmos. Chem. Phys., 24, 14101–14122, https://doi.org/10.5194/acp-24-14101-2024, 2024.

He, B.-J.: Potentials of meteorological characteristics and synoptic conditions to mitigate urban heat island effects, Urban Climate, 24, 26–33, https://doi.org/10.1016/j.uclim.2018.01.004, 2018.

Heaviside, C., Cai, X. -M., and Vardoulakis, S.: The effects of horizontal advection on the urban heat island in Birmingham and the West Midlands, United Kingdom during a heatwave, Quart J Royal Meteoro Soc, 141, 1429–1441, https://doi.org/10.1002/qj.2452, 2015.

Hong, S.-Y., Noh, Y., and Dudhia, J.: A New Vertical Diffusion Package with an Explicit Treatment of Entrainment Processes, Monthly Weather Review, 134, 2318–2341, https://doi.org/10.1175/MWR3199.1, 2006.

Huang, X., Li, J., Yang, J., Zhang, Z., Li, D., and Liu, X.: 30 m global impervious surface area dynamics and urban expansion pattern observed by Landsat satellites: From 1972 to 2019, Sci. China Earth Sci., 64, 1922–1933, https://doi.org/10.1007/s11430-020-9797-9, 2021.

Janjić, Z. I.: The Step-Mountain Eta Coordinate Model: Further Developments of the Convection, Viscous Sublayer, and Turbulence Closure Schemes, Mon. Wea. Rev., 122, 927–945, https://doi.org/10.1175/1520-0493(1994)122%3C0927:TSMECM%3E2.0.CO;2, 1994.

https://doi.org/10.5194/egusphere-2026-1707
Preprint. Discussion started: 14 April 2026

Kittner, J., Fenner, D., Demuzere, M., and Bechtel, B.: Analysis of nocturnal urban heat advection using crowd weather stations, Quart J Royal Meteoro Soc, 151, e5065, https://doi.org/10.1002/qj.5065, 2025.

Lowry, W. P.: Empirical Estimation of Urban Effects on Climate: A Problem Analysis, J. Appl. Meteor., 16, 129–135, https://doi.org/10.1175/1520-0450(1977)016%3C0129:EEOUEO%3E2.0.CO;2, 1977.

Lu, H., Zhang, M., Sun, W., and Li, W.: Expansion Analysis of Yangtze River Delta Urban Agglomeration Using DMSP/OLS Nighttime Light Imagery for 1993 to 2012, IJGI, 7, 52, https://doi.org/10.3390/ijgi7020052, 2018.

Mahrt, L.: Stably Stratified Atmospheric Boundary Layers, Annual Review of Fluid Mechanics, 46, 23–45, https://doi.org/10.1146/annurev-fluid-010313-141354, 2014.

Meng, F., Guo, J., Ren, G., Zhang, L., and Zhang, R.: Impact of urban heat island on the variation of heating loads in residential and office buildings in Tianjin, Energy and Buildings, 226, 110357, https://doi.org/10.1016/j.enbuild.2020.110357, 2020.

Mlawer, E. J., Taubman, S. J., Brown, P. D., Iacono, M. J., and Clough, S. A.: Radiative transfer for inhomogeneous atmospheres: RRTM, a validated correlated-k model for the longwave, J. Geophys. Res., 102, 16663–16682, https://doi.org/10.1029/97JD00237, 1997.

Moustaoui, M. and Georgescu, M.: Winds of Change: The Role of Urban Expansion and Thermal Advection in Driving Phoenix's (AZ) Warming Trends, JGR Atmospheres, 130, e2024JD043166, https://doi.org/10.1029/2024JD043166, 2025.

Oke, T. R.: City size and the urban heat island, Atmospheric Environment (1967), 7, 769–779, https://doi.org/10.1016/0004-6981(73)90140-6, 1973.

Oke, T. R.: The distinction between canopy and boundary-layer urban heat islands, Atmosphere, 14, 268–277, https://doi.org/10.1080/00046973.1976.9648422, 1976.

Oke, T. R., Mills, G., Christen, A., and Voogt, J. A.: Urban Climates, 1st ed., Cambridge University Press, https://doi.org/10.1017/9781139016476, 2017.

Phelan, P. E., Kaloush, K., Miner, M., Golden, J., Phelan, B., Silva, H., and Taylor, R. A.: Urban Heat Island: Mechanisms, Implications, and Possible Remedies, Annu. Rev. Environ. Resour., 40, 285–307, https://doi.org/10.1146/annurev-environ-102014-021155, 2015.

Qian, J., Zhang, L., Schlink, U., Meng, Q., Liu, X., and Janscó, T.: High spatial and temporal resolution multi-source anthropogenic heat estimation for China, Resources, Conservation and Recycling, 203, 107451, https://doi.org/10.1016/j.resconrec.2024.107451, 2024.

Shi, T., Yang, Y., Qi, P., Ren, G., Wen, X., and Gul, C.: Adjustment of the urbanization bias in surface air temperature series based on urban spatial morphologies and using machine learning, Urban Climate, 55, 101991, https://doi.org/10.1016/j.uclim.2024.101991, 2024.

Shi, T., Yang, Y., Zong, L., Guo, M., Qi, P., and Lolli, S.: The modulation of synoptic weather patterns and human activities on the diurnal cycle of the summertime canopy urban heat island in the Yangtze River Delta Urban Agglomeration, China, Atmos. Chem. Phys., 25, 4989–5007, https://doi.org/10.5194/acp-25-4989-2025, 2025.

Silva, R., Carvalho, A. C., Carvalho, D., and Rocha, A.: Study of Urban Heat Islands Using Different Urban Canopy Models and Identification Methods, Atmosphere, 12, 521, https://doi.org/10.3390/atmos12040521, 2021.

https://doi.org/10.5194/egusphere-2026-1707
Preprint. Discussion started: 14 April 2026

Stull, R. B. (Ed.): An Introduction to Boundary Layer Meteorology, Springer Netherlands, Dordrecht, https://doi.org/10.1007/978-94-009-3027-8, 1988.

Sun, J., Mahrt, L., Banta, R. M., and Pichugina, Y. L.: Turbulence Regimes and Turbulence Intermittency in the Stable Boundary Layer during CASES-99, Journal of the Atmospheric Sciences, 69, 338–351, https://doi.org/10.1175/JAS-D-11-082.1, 2012.

Tewari, M., Chen, F., Wang, W., Dudhia, J., LeMone, M. A., Mitchell, K., Ek, M., Gayno, G., Wegiel, J., and Cuenca, R. H.: Implementation and verification of the unified NOAH land surface model in the WRF model, 20th conference on weather analysis and forecasting/16th conference on numerical weather prediction, 11–15, 2004.

Thompson, G., Field, P. R., Rasmussen, R. M., and Hall, W. D.: Explicit Forecasts of Winter Precipitation Using an Improved Bulk Microphysics Scheme. Part II: Implementation of a New Snow Parameterization, Monthly Weather Review, 136, 5095–5115, https://doi.org/10.1175/2008MWR2387.1, 2008.

Tian, G., Jiang, J., Yang, Z., and Zhang, Y.: The urban growth, size distribution and spatio-temporal dynamic pattern of the Yangtze River Delta megalopolitan region, China, Ecological Modelling, 222, 865–878, https://doi.org/10.1016/j.ecolmodel.2010.09.036, 2011.

Tian, W., Yang, Y., Wang, L., Zong, L., Zhang, Y., and Liu, D.: Role of local climate zones and urban ventilation in canopy urban heat island–heatwave interaction in Nanjing megacity, China, Urban Climate, 49, 101474, https://doi.org/10.1016/j.uclim.2023.101474, 2023.

Wang, L., Fan, S., Hu, F., Miao, S., Yang, A., Li, Y., Liu, J., Liu, C., Chen, S., Ho, H. C., Duan, Z., Gao, Z., and Yang, Y.: Vertical Gradient Variations in Radiation Budget and Heat Fluxes in the Urban Boundary Layer: A Comparison Study Between Polluted and Clean Air Episodes in Beijing During Winter, JGR Atmospheres, 125, e2020JD032478, https://doi.org/10.1029/2020JD032478, 2020.

Wong, K. K. and Dirks, R. A.: Mesoscale Perturbations on Airflow in the Urban Mixing Layer, J. Appl. Meteor., 17, 677–688, https://doi.org/10.1175/1520-0450(1978)017%3C0677:MPOAIT%3E2.0.CO;2, 1978.

Xian, J., Luo, H., Lu, C., Lin, X., Yang, H., and Zhang, N.: Characteristics of the atmospheric boundary layer height: A perspective on turbulent motion, Science of The Total Environment, 919, 170895, https://doi.org/10.1016/j.scitotenv.2024.170895, 2024.

Xue, J., Zong, L., Yang, Y., Bi, X., Zhang, Y., and Zhao, M.: Diurnal and interannual variations of canopy urban heat island (CUHI) effects over a mountain–valley city with a semi-arid climate, Urban Climate, 48, 101425, https://doi.org/10.1016/j.uclim.2023.101425, 2023.

Xue, J., Zhang, L., Wang, L., Baklanov, A., and Yang, Y.: Characteristics and Mechanisms of Non-Stationary Turbulence in a Megacity Area, Geophysical Research Letters, 52, e2025GL114978, https://doi.org/10.1029/2025GL114978, 2025.

Yang, Y., Zheng, Z., Yim, S. Y. L., Roth, M., Ren, G., Gao, Z., Wang, T., Li, Q., Shi, C., Ning, G., and Li, Y.: $PM_{2.5}$ Pollution Modulates Wintertime Urban Heat Island Intensity in the Beijing-Tianjin-Hebei Megalopolis, China, Geophysical Research Letters, 47, https://doi.org/10.1029/2019GL084288, 2020.

Yang, Y., Guo, M., Wang, L., Zong, L., Liu, D., Zhang, W., Wang, M., Wan, B., and Guo, Y.: Unevenly spatiotemporal distribution of urban excess warming in coastal Shanghai megacity, China: Roles of geophysical environment, ventilation and sea breezes, Building and Environment, 235, 110180, https://doi.org/10.1016/j.buildenv.2023.110180, 2023.

https://doi.org/10.5194/egusphere-2026-1707
Preprint. Discussion started: 14 April 2026

Yao, L., Sailor, D. J., Yang, X., Xu, G., and Zhao, L.: Are water bodies effective for urban heat mitigation? Evidence from field studies of urban lakes in two humid subtropical cities, Building and Environment, 245, 110860, https://doi.org/10.1016/j.buildenv.2023.110860, 2023.

Zhang, D., Shou, Y., and Dickerson, R. R.: Upstream urbanization exacerbates urban heat island effects, Geophysical Research Letters, 36, 2009GL041082, https://doi.org/10.1029/2009GL041082, 2009.

Zhang, L., Zhang, H., Zhang, X., Li, Q., Wu, B., Cai, X., Song, Y., and Zhu, T.: Dissimilarity of Turbulent Transport of Momentum and Heat Under Unstable Conditions Linked to Convective Circulations, Journal of Geophysical Research: Atmospheres, 128, e2022JD037997, https://doi.org/10.1029/2022JD037997, 2023.

Zhang, L., Luo, F., Pan, G., Zhang, W., Ren, G., Zheng, Z., and Yang, Y.: Elucidating the Multi-Timescale Variability of a Canopy Urban Heat Island by Using the Short-Time Fourier Transform, Geophysical Research Letters, 51, e2023GL106221, https://doi.org/10.1029/2023GL106221, 2024a.

Zhang, L., Zhang, H., Cai, X., Song, Y., and Zhang, X.: Characteristics of Turbulence Intermittency, Fine Structure, and Flux Correction in the Taklimakan Desert, Journal of the Atmospheric Sciences, 81, 459–475, https://doi.org/10.1175/JAS-D-23-0107.1, 2024b.

Zhao, Y., Zhong, L., Ma, Y., Fu, Y., Chen, M., Ma, W., Zhao, C., Huang, Z., and Zhou, K.: WRF/UCM simulations of the impacts of urban expansion and future climate change on atmospheric thermal environment in a Chinese megacity, Climatic Change, 169, 38, https://doi.org/10.1007/s10584-021-03287-7, 2021.

Zheng, Z., Ren, G., Gao, H., and Yang, Y.: Urban ventilation planning and its associated benefits based on numerical experiments: A case study in beijing, China, Building and Environment, 222, 109383, https://doi.org/10.1016/j.buildenv.2022.109383, 2022.

Zheng, Z., Luo, F., Li, N., Gao, H., and Yang, Y.: Impact of Local Climate Zones on the Urban Heat and Dry Islands in Beijing: Spatial Heterogeneity and Relative Contributions, J Meteorol Res, 38, 126–137, https://doi.org/10.1007/s13351-024-3081-6, 2024.

Zhou, D., Bonafoni, S., Zhang, L., and Wang, R.: Remote sensing of the urban heat island effect in a highly populated urban agglomeration area in East China, Science of The Total Environment, 628–629, 415–429, https://doi.org/10.1016/j.scitotenv.2018.02.074, 2018.

Zhu, D. and Ooka, R.: WRF-based scenario experiment research on urban heat island: A review, Urban Climate, 49, 101512, https://doi.org/10.1016/j.uclim.2023.101512, 2023.

Zong, L., Yang, Y., Gao, M., Wang, H., Wang, P., Zhang, H., Wang, L., Ning, G., Liu, C., Li, Y., and Gao, Z.: Large-scale synoptic drivers of co-occurring summertime ozone and $PM_{2.5}$ pollution in eastern China, Atmos. Chem. Phys., 21, 9105–9124, https://doi.org/10.5194/acp-21-9105-2021, 2021.